Implicit large eddy simulations for hydrodynamic stress characterization in 125mL shake flasks for stem cell cultures

van Valderen, Ramon D.; Juarez-Garza, Brenda E.; Klijn, Marieke E.; Ottens, Marcel; Haringa, Cees

DOI
10.1016/j.bej.2025.109734

Publication date
2025

Document Version
Final published version

Published in
Biochemical Engineering Journal

Citation (APA)
van Valderen, R. D., Juarez-Garza, B. E., Klijn, M. E., Ottens, M., & Haringa, C. (2025). Implicit large eddy simulations for hydrodynamic stress characterization in 125mL shake flasks for stem cell cultures. *Biochemical Engineering Journal*, *219*, Article 109734. https://doi.org/10.1016/j.bej.2025.109734

Biochemical Engineering Journal 219 (2025) 109734

Contents lists available at ScienceDirect

Biochemical Engineering Journal

journal homepage: www.elsevier.com/locate/bej

Implicit large eddy simulations for hydrodynamic stress characterization in 125 mL shake flasks for stem cell cultures

Ramon D. van Valderen [1], Brenda E. Juarez-Garza [2], Marieke E. Klijn [3], Marcel Ottens, Cees Haringa [*,4]

Delft University of Technology, Van Der Maasweg 9, Delft, Zuid-Holland 2629 Hz, the Netherlands

ARTICLE INFO

Keywords:
Computational fluid dynamics
Lattice Boltzmann method
Implicit large Eddy simulations
Stem cell cultures
Shake flasks
Hydrodynamic stress

ABSTRACT

Cell therapies based on inducible pluripotent stem cells offer promising new treatments for a variety of different illnesses. However, the sensitivity of stem cells to hydrodynamic stress makes developing reliable stem cell production processes challenging. Understanding hydrodynamic stress conditions experienced by stem cells during early-stage process development is important to guide scale-up and design scale-down experiments. We characterize the hydrodynamic stresses in a 125 mL shake flask using Lattice-Boltzmann implicit large eddy simulations (LB-ILES). First, we validated the LB-ILES shake flask simulations using volumetric power input measurements and experimental liquid distribution data showing good overall agreement, while also numerical challenges of the LB-ILES method regarding grid and time step dependencies are discussed. The mean shear stress in the shake flask increases from 0.01 to 0.24 Pa when increasing the shaking frequency from 55 to 250 rpm, and the mean Kolmogorov length scale decreases from 185 to 51 μm. Furthermore, time-averaged distributions of the shear stress and Kolmogorov length scales were evaluated and compared to reported stress thresholds for stem cells. Based on the shear stress and Kolmogorov length scale distributions, our developed shake flask CFD model can help to design small-scale experiments to characterize stem cell cultures in terms of their hydrodynamic stress tolerance, and ultimately guide scale-up stem cell cultures to larger cultivation systems.

1. Introduction

Human inducible pluripotent stem cells (iPSC) hold great potential for the development of new stem cell-based therapies to treat many illnesses, such as Parikinson's, multiple sclerosis (MS), and sickle cell disease [1–3]. To obtain a sufficient number of cells for such therapies, upscaling of the stem cell production process is needed under well-defined process conditions [4]. In recent years, protocols emerged to expand and differentiate iPSCs in a well-controlled manner by creating embryoid bodies (EBs), which are 3D iPSC aggregates with the ability to differentiate into cells of all three germ layers [5,6]. Stem cell production through 3D aggregates (e.g., EBs, spheroids or adherent cells to microcarries) enables the cultivation in stirred-tank bioreactors as a suspension culture, allowing tight control of process variables such as pH, temperature, and dissolved oxygen concentration [7]. However, scaling up stem cell production to large-scale bioreactors remains challenging, in particular due to the sensitivity of stem cell cultures to hydrodynamic stress. [8–11]. Unfortunately, it becomes prohibitively expensive to evaluate different process operating conditions at production scale, especially due to the high associated media costs of iPSC cultures [12]. It would therefore be useful to have simple lab-scale experiments to assess the sensitivity of stem cell cultures to hydrodynamic stress, which translate easily across scales.

Shake flasks are an example of a commonly used lab-scale system in cell cultures, due to their ease of operation and low costs [13]. Aglialoro et al. [14] showed that shake flasks can generate sufficient hydrodynamic stress to induce a strong mechanosensor stress response in single cell erythroblasts cultures, and could therefore be suited systems for scaled-down hydrodynamic stress sensitivity experiments. However, the translation of operating conditions from shake flask to stirred-tank

* Corresponding author.
E-mail address: c.haringa@tudelft.nl (C. Haringa).
[1] 0009–0001-8585–6478.
[2] 0009–0007-7026–9901.
[3] 0000–0001-5203–4649.
[4] 0000–0003-0310–1045.

https://doi.org/10.1016/j.bej.2025.109734
Received 24 January 2025; Received in revised form 14 March 2025; Accepted 25 March 2025
Available online 27 March 2025

bioreactor is not trivial, as the mechanism to induce fluid motion is fundamentally different. This means it is important to understand the local hydrodynamic conditions in shake flasks, and how the shake flask's operating conditions (e.g., shaking frequency) modulate the hydrodynamic stress experienced by cells. This ensures the basis for a fundamentally sound approach to design a scale-down experiment using shake flasks to approximate the hydrodynamic stress of large-scale cultivation systems, such as stirred-tank bioreactors.

The importance of the hydrodynamic characterization of shake flasks has been acknowledged. For example, different mathematical models were developed to describe the fluid motion in shake flasks [15,16]. Furthermore, Büchs et al. [17] developed a set of empirical correlations to determine sensible shake flask operating conditions based on dimensionless numbers, namely the shake flasks' Reynolds number (Re) and Phase number (Ph). These models and empirical correlations allow for a quick estimate of important engineering parameters, such as mass transfer and power consumption, but are unable to quantify local hydrodynamic stresses inside the shake flask.

Computational fluid dynamics (CFD) is a numerical technique to simulate complex fluid flows, and can be used to obtain a detailed and local description of a fluid, from which important hydrodynamic stress parameters can be determined. In the bioprocess industry, CFD simulations are nowadays used routinely to characterize stirred-tank bioreactors [18–20]. Although less common, CFD has also been applied to characterize the flow in shake flasks, mostly focusing on mass transfer, volumetric power input, and shear rates [21–23]. Liu et al. [24] performed an analysis of hydrodynamic stress in shake flasks using CFD for plant cell suspension cultures, where calculations of shear damage on large diameter plant aggregates were included. Dinter et al. [23] developed a 250 mL shake flask CFD model and extensively validated their model on experimental data of liquid heights and volumetric power inputs at water-like (1 mPa·s) and moderate viscosities (16 mPa·s). In follow-up work, Dinter et al. [25] extended the validation to liquids with high viscosity (100 mPa · s). However, all of these CFD studies focused on larger shake flasks with volumes between 250 and 500 mL, with shaking diameters between 25 and 50 mm. Consequently, due to the larger shake flask size and shaking diameter, most of these studies focus on more turbulent flow conditions ($Re > 25,000$), which are typically avoided when cultivating iPSCs and EBs. For such stem cell cultures, typically smaller shake flasks with smaller shaking diameters are used to avoid such turbulent flow conditions, as well as to reduce the required amount of expensive media.

Next to the lack of relevance of the previous work to cell cultures, all aforementioned CFD shake flask models are based on Finite Volume (FV) Reynolds Averaged Navier Stokes (RANS) models. Although powerful and well-established, FV methods require significant computational resources as the computations can only be parallelized to a certain degree. To reduce computational costs, FV methods are often combined with RANS-based turbulence models, which only provide a time-averaged turbulence representation of the Navier-Stokes equations. Consequently, temporal turbulence fluctuations cannot be captured including, for example, short-term fluctuations in shear stresses that might affect cultivation of iPSCs or EBs. Moreover, deciding which RANS-based turbulence model is most suited for modeling fluid flow in a shake flask is not obvious, as previous studies have used a variety of RANS-based turbulence models including standard k-epsilon, RNG k-epsilon and k-omega SST [21–24].

Recently, the Lattice Boltzmann (LB) method has gained more traction for simulating fluid flows, as its parallelizable numerical scheme results in fast computation times on modern graphics processing units (GPUs). Rather than discretizing the Navier-Stokes equations directly, as done in the FV method, the LB method discretizes the Boltzmann equation from which the macroscopic incompressible Navier-Stokes equations can be recovered [26]. Nowadays, a variety of available LB code implementations exist including open-source, such as OpenLB, as well as commercial codes, such as M-Star CFD. The speedup of LB codes over more traditional FV-RANS methods allows for the more routine use of highly resolved turbulence models such as large eddy simulations (LES), which has the ability to explicitly capture more details of the turbulent energy spectrum. This speedup also makes it easier to simulate longer process times and add more complex physics. These advanced capabilities are reflected by the use of LB-LES for stirred-tank bioreactors to simulate free surface oxygen transfer, particle suspension, and proportional-integral-derivative (PID) controller functionalities [27–29]. Haringa [30] used LB-LES to simulate cellular lifelines in an industrial-scle stirred tank bioreactor, which enabled simulation of many Lagrangian particles at tractable computational times. Šrom et al. [31] used LB-LES to determine the maximum hydrodynamic stress at different bioreactor scales for mammalian cell cultures and experimentally validated the simulations using shear sensitive micro-probes. LB-LES could be used in a similar manner to simulate shake flasks fluid flow for cell culture processes by investigating, for example, hydrodynamic stresses, oxygen transfer, and cellular lifelines. However, to our knowledge, LB-LES has not yet been used to simulate shake flask fluid flows.

Accurately capturing the free surface dynamics becomes important when simulating shake flask fluid flow, and requires extension of the LB framework to handle multiphase systems. Many multiphase LB methods exist that deal with modeling the internal interfaces between two immiscible fluids [32]. Traditionally, LB-CFD has difficulties simulating high-density and high viscosity ratios. Given that most cell culture media have properties close to water, simulating a shake flask requires an LB method that can handle such high density (≈ 1000) and viscosity (≈ 70) ratios. Fortunately, many advances have been made to improve stability of multiphase LB methods. For example, Sitompul and Aoki [33] proposed a multi-phase LB method to simulate two-phase flows at high density and viscosity ratios, and at high Reynolds numbers ($> 10^5$) which requires numerical stability at fast topological changes of the interface. Their LB method (CPH-CM-LB) uses a cumulant collision model (CM) to improve stability, combined with a conservative phase-field (CPH) LB method for interface capturing [34,35]. In addition, Sitompul and Aoki [33] included second-order filters for the pressure and velocity fields to improve stability. Since the flow in shake flasks generally does not exceed Reynolds numbers above 40,000; the CPH-CM-LB method should be more than capable to simulate two-phase shake flask flow. Recently, the CPH-CM-LB method based on the work of Sitompul and Aoki [33] has been made available in the commercial software M-Star CFD.

Interestingly, in the cumulant-based LB method by Geier et al. [34], and later further improved by Geier et al. [36], no explicit turbulence model is added. This means that all missing sub-grid scale dissipation is introduced by selective damping of small-scale fluctuations, which happens primarily through the relaxation mechanism of higher-order cumulants. When additional implicit filters of the pressure and velocity fields are used, as done by Sitompul and Aoki [33], even more numerical dissipation is introduced. The introduction of all sub-grid dissipation by the numerical truncation error is known as implicit large eddy simulations (ILES) [37]. This is contrary to standard LES where the sub-grid dissipation is added explicitly by a physically motivated turbulent viscosity. The advantage of ILES in LB frameworks is that implementation is straightforward and does not require additional sub-grid-scale equations to be solved, thus making it computationally more efficient. However, tuning of the relaxation rate and filter parameters is often done heuristically without any particular physical basis. Furthermore, the relaxation rate and filter parameters are directly coupled to the grid and time resolution, meaning that the LB-ILES simulated dissipation might be grid and time step dependent. Consequently, it is not guaranteed that the dissipation introduced by LB-ILES scales appropriately with the turbulent energy cascade. Therefore, it is important to quantitatively validate LB-ILES with experimental data. Currently, no quantitative validation studies on energy dissipation exist for two-phase LB-ILES [33], and only a limited number of quantitative

validation studies on energy dissipation exist for single-phase LB-ILES [36,38].

Here, we analyze the hydrodynamic stresses inside 125 mL shake flasks at moderate Reynolds numbers ($Re \approx 5000–25{,}000$), a setup regularly used for early-stage scale-up experiments for EB-based cultivation processes [39–41]. To simulate the two-phase shake flask fluid flow, we used the novel CPH-CM-LB-ILES model of M-Star CFD to simulate two-phase shake flask fluid flow. For simplicity, in this text we will refer to this CPH-CM-LB-ILES method as simply LB-ILES.

We first validated the two-phase LB-ILES approach for modeling shake flask flow. We considered careful validation critical, given the relative novelty of the used LB-ILES method, and since only a limited amount of studies have focused on quantitatively validating this method. Therefore, we first simulated a 250 mL shake flask and compared it to already existing mean energy dissipation rate reference data, covering a wide range of Reynolds numbers ($Re = 1250 - 40,000$). Subsequently, we assessed the quality of our 125 mL shake flask of interest using an empirical correlation for the mean energy dissipation rate, and by comparing the simulated liquid distributions with experimental liquid distributions. Based on this quantitative validation the accuracy and challenges of two-phase LB-ILES are discussed in more detail, specifically regarding grid and time step dependencies.

After model validation, we analyzed the hydrodynamic stresses inside the 125 mL shake flask by comparing the shear stress distributions (τ) and Kolmogorov length scales (λ_k) for a range of different shaking frequencies, and compared those to reported stem cell cultivation conditions in literature. To conclude, we reflect on the possibilities and challenges that LB-ILES methods offer for accurately simulating shake flask fluid flows, and how such methods to quantify hydrodynamic stresses help in scaling up stem cell culture processes.

2. Material and methods

2.1. Flask setup

The shake flask studied in this work was a 125 mL shake flask with a maximum inner shake flask diameter of 63.5 mm (Fig. 1). During the simulations, the shaking diameter was set at 19 mm with a filling volume of 12.5 mL (10 % WV). The shaking frequencies were varied between 55 and 250 rpm.

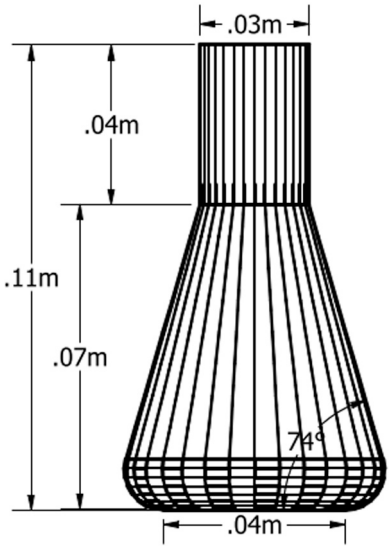

Fig. 1. Geometry of 125 mL shake flask.

2.2. Immiscible two-fluid flow simulations

We used M-Star CFD software v3.11.33 to simulate the two-phase fluid flow, which uses the Lattice-Boltzmann (LB) method to solve the incompressible Navier-Stokes equations:

$$\nabla u = 0, \tag{1}$$

$$\frac{\partial u}{\partial t} + u \cdot \nabla u = \nu \nabla^2 u + g - \frac{\nabla p}{\rho} + \frac{1}{\rho} f_b + \frac{1}{\rho} f_s. \tag{2}$$

Here, the local fluid velocity at time t is described by u, the gravitational acceleration by g, the pressure by p, the fluid density by ρ, the fluid kinematic viscosity by ν, the body force density by f_b and the surface tension force per unit mass by f_s. The software numerically solves the lattice Boltzmann equation:

$$f_i(x + c_i \Delta t, t + \Delta t) = f_i(x, t) + \Omega_i(x, t). \tag{3}$$

This describes the fluid as a set of discrete particles distributions $f_i(x, t)$, which move with velocity c_i to a neighboring lattice point $x + c_i \Delta t$ at the next time step $t + \Delta t$, which is called the streaming step. At the same time, particles are redistributed among the populations f_i during the collision step via the collision operator $\Omega_i(x,t)$ [26]. In M-Star CFD, we chose to model both the liquid and gas phase explicitly using the Immiscible Two Fluid (ITF) model with the High Density Ratio (ITF-HDR) option enabled. This was motivated by our observations that M-Star CFD's Free Surface (FS) model, where the fluid dynamics of the empty space are not modeled explicitly, resulted in incorrect fluid behavior (see Figure A.10 of the supporting information). The model uses a cumulant based collision operator to relax f_i to its equilibrium state f_i^{eq} [34]. M-Star's ITF-HDR model includes additional improvements of the cumulant lattice Boltzmann method as described in Geier et al. [36], which include optimized relaxation rate parameters to obtain fourth order accurate diffusion (section 5 in Geier et al. [36]) and relaxation rate limiter (section 6 in Geier et al. [36]) to improve stability.

The interface tracking is done using a conservative phase-field lattice Boltzmann method based on the Allen-Cahn equation [35,42]. The two fluids are modeled as a single fluid where the density ρ and kinematic viscosity ν are defined using

$$\rho = \rho_1 + \phi(\rho_2 - \rho_1), \tag{4}$$

$$\nu = \nu_1 + \phi(\nu_2 - \nu_1). \tag{5}$$

Here, ϕ is an order parameter that distinguishes the two fluids (subscripts 1 and 2, respectively). The interface between the gas and liquid phase is described by the spatio-temporal evolution of ϕ using:

$$\frac{\partial \phi}{\partial t} + \nabla \cdot \phi u = \nabla \left[M \left(\nabla \phi - \frac{1 - 4\left(\phi - \frac{1}{2}\right)^2}{W} \right) n \right], \tag{6}$$

where M is the mobility parameter, W the interface width and n the normal vector.

During the simulation the energy dissipation ε is calculated using:

$$\varepsilon = 2\nu \sum_{i,j} \bar{S}_{ij} \bar{S}_{ij}. \tag{7}$$

Here, ν is the fluid kinematic viscosity and $\bar{S}_{i,j}$ the norm of the resolved strain rate tensor. In the LB method, the strain rate tensor $S_{i,j}$ can be obtained locally from the second order cumulants, as described in [36].

In this work, the liquid phase was assumed to have water-like properties at 37°C with a density of 993 kg/m^3 and kinematic viscosity of $6.96 \cdot 10^{-7}$ m^2/s. The modeled gas phase had air-like properties with a density of 1.138 kg/m^3 and kinematic viscosity of $1.67 \cdot 10^{-5}$ m^2/

s. The gravitational constant was set at 9.81 m^2/s, and surface tension at 0.07 N/m.

We used M-Star CFD's Orbital Shaking acceleration function to model the shake flask motion, which adds a cyclic centrifugal acceleration to each fluid element on the x-z plane based on its position and time [24]:

$$a_x = \omega^2 r \cdot cos(\omega t), \tag{8}$$

$$a_z = \omega^2 r \cdot sin(\omega t), \tag{9}$$

where ω describes the angular velocity, r the radius of the shaker motion and t the time.

Similarly as in the work of Sitompul and Aoki [33], a D3Q27 lattice was used which is needed for stability. To reduce computational costs, only part of the shake flask geometry was used during the simulations by filling the domain with lattice points up until a height of 4 cm. A no-slip boundary condition was used at the shake flask wall. At the top of the lattice domain, where the gas phase starts, a pressure boundary was defined using 101,325 Pa. All boundaries were set to grid-aligned half-way bounce-back boundaries. Based on the grid dependence study, we found that 40 million lattice points (400 lattice points across shake flask diameter), with a Courant number of 0.01, was optimal in terms of simulation accuracy. A standard desktop containing an NVIDIA RTX3090 24 GB GPU was used for all simulations, which enabled an average computational speed of 0.125 s of simulation time per hour of computational time. Data post-processing was done using Python 3.9.16 and Paraview 5.10.1.

2.3. Energy dissipation rate correlation

In unbaffled shake flasks, the average energy dissipation rate ($\bar{\varepsilon}$) may be calculated using the correlation of [43]:

$$\bar{\varepsilon} = Ne' \cdot n^3 \cdot d^4 \cdot V_L^{-2/3}, \tag{10}$$

where n is the shaking frequency in s^{-1}, d the maximum inside shaking flask diameter in m, V_L the filling volume in m^3. The modified power number Ne' can be determined with:

$$Ne' = 70 \cdot Re^{-1} + 25 \cdot Re^{-0.6} + 1.5 \cdot Re^{-0.2}, \tag{11}$$

where,

$$Re = \frac{\rho \cdot n \cdot d^2}{\mu}, \tag{12}$$

where ρ is the fluid density in kg/m^3 and μ the dynamic fluid viscosity in Pa · s.

2.4. Energy dissipation rate calculations from simulations

For each lattice point i, the local energy dissipation rate in the liquid phase ($\varepsilon_{L,i}$) is determined by:

$$\varepsilon_{L,i} = \varepsilon_i \cdot f_{L,i}, \tag{13}$$

where ε_i is the total energy dissipation rate and $f_{L,i}$ the liquid volume fraction in the lattice point. We then calculated the mean energy dissipation rate in the liquid phase $\overline{\varepsilon_L}$ using the weighted average of each cell with respect to each volume fraction:

$$\overline{\varepsilon_L} = \frac{\sum_i \varepsilon_i \cdot f_{L,i}}{\sum f_{L,i}}. \tag{14}$$

The value of $\overline{\varepsilon_L}$ was determined for each transient simulation after pseudo steady-state of ε was reached. To simplify, we will refer to $\overline{\varepsilon_L}$ with $\bar{\varepsilon}$ as only the energy dissipation in the liquid phase is of interest in this work.

The mean energy dissipation rate $\bar{\varepsilon}$ is related to the volumetric power input $\frac{P}{V_L}$ by:

$$\bar{\varepsilon} \cdot \rho = \frac{P}{V_L}, \tag{15}$$

where P is the total power input in J/s. Equation (15) is used to compare the simulation results to the volumetric power input measurements by Dinter et al. [23].

2.5. Hydrodynamic stress calculations from simulations

The viscous stress tensor $\tau_{i,j}$ is determined from the strain rate tensor using:

$$\tau_{i,j} = 2\rho\nu S_{i,j}. \tag{16}$$

The shear stress magnitude τ_{shear} is then determined by computing the Euclidean norm of the off-diagonal terms of the viscous stress tensor:

$$\tau_{shear} = \sqrt{\sum_{i \neq j} \tau_{i,j}^2}. \tag{17}$$

The Kolmogorov length scale is defined as:

$$\lambda_k = \left(\frac{\nu^3}{\varepsilon}\right)^{1/4}, \tag{18}$$

where ν is the fluid kinematic viscosity and ε the local energy dissipation rate. To obtain distributions of τ and λ_k, simulation data from 2 full rotations, with 8 sample times per rotation, were combined and used to determine the distributions. The simulation data was collected after 2 s of flow time, so that the shake flask fluid flow reached pseudo steady-state. We used a liquid volume fraction f_L cutoff larger than 0.5 to construct the distributions, as values close to the liquid interface $f_L < 0.5$ exhibited nonphysically high values in some cases, which is likely caused by numerical inaccuracies.

2.6. Shake flask liquid distribution experiments

To experimentally validate the predicted liquid distributions, an unbaffled polycarbonate shake flask with a total volume of 125 mL (Corning, New York, United States of America) was agitated on an orbital shaker with a 19 mm shaking diameter (Thermo Fisher Scientific Inc., Waltham, United States of America). We used a digital photo camera (Canon, Japan) to capture the liquid distribution inside the shake flask at various time points. To increase the contrast, the water was stained with black food coloring.

2.7. Simulations of 250 mL shake flask

For LB-ILES validation, we simulated a 250 mL shake flask with both a filling volume of 25 mL and 40 mL and a kinematic fluid viscosity of both 1 and 16 mm^2/s. Shaking frequencies were varied between 180 and 380 rpm using a shaking diameter of 25 mm and a contact angle of 20 degrees. The glass shake flask geometry and all other physical parameters were kept identical to the simulations performed by Dinter et al. [23]. For this system, we found that 34.1 million lattice points (400 lattice points across the shake flask diameter) with a Courant number of 0.01, at a maximum domain height of 4.5 cm, was optimal in terms of accuracy.

3. Results

3.1. LB-LES model validation using experimental data of a 250 mL shake flask

For validation of the LB-ILES method, we compared simulations of a 250 mL shake flask to experimental and simulated volumetric power

input (P/V) data reported by Dinter et al. [23]. We use this data to validate the LB-ILES simulated mean energy dissipation rate ($\bar{\varepsilon}$) using its relation with the volumetric power input (Equation 15) for different shaking frequencies from 180 to 380 rpm, kinematic viscosities of 1 and 16 mm^2/s and a filling volume of 25 mL (Fig. 2).

For the higher viscosity of 16 mm^2/s (Re ≈ 1250–2500), the LB-ILES simulated $\bar{\varepsilon}$ aligns closely to the measured $\bar{\varepsilon}$ by Dinter et al. [23], with an average deviation of 0.40 W/kg (relative deviation of 10.8 %) (Fig. 2B). We also compared our LB-ILES simulations to the Finite Volume (FV) k-omega SST simulations from Dinter et al. [23] (Fig. 2; square symbols), which showed an even closer agreement with our model with a mean deviation of 0.18 W/kg (relative deviation of 3.8 %). For simulations at a viscosity of 1 mm^2/s (Re ≈ 20,000–40,000), the predicted $\bar{\varepsilon}$ is again in close agreement with the reference data (Fig. 2A). Only at $Re > 37,000$, a slight under-prediction of $\bar{\varepsilon}$ was observed. For this low water-like viscosity, the LB-ILES simulated $\bar{\varepsilon}$ had an average deviation of 0.18 W/kg (relative deviation of 21.6 %) from the measurements of Dinter et al. [23] and 0.15 W/kg from the simulations of Dinter et al. [23] (relative deviation of 13.2 %). For both viscosities, the empirical correlation of Büchs et al. [43] correlates well with our simulations and the work of Dinter et al. [23], demonstrating the usefulness and accuracy of this correlation for a wide range of operating conditions. Similar agreement of our simulation data with the reference data was found for a higher filling volume, demonstrating the capabilities of LB-ILES to simulate a wide range of shake flask operating conditions (40 mL, see Figure A.11 of the supporting information).

However, grid convergence was not yet observed for the simulations at a water-like viscosity of 1 mm^2/s. At $Re \approx 40,000$, refining the grid further helps to bring $\bar{\varepsilon}$ closer to the reference data, which would suggest that the LB-ILES simulations were insufficiently resolved to capture most of ε at these flow conditions (Fig. 3C). A similar grid dependence was observed at $Re \approx 20,000$, even though in this case the simulated $\bar{\varepsilon}$ was already close to the reference data and further grid refinement seemed to result in over-prediction of $\bar{\varepsilon}$ (Fig. 3B). Moreover, in both cases reducing the grid spacing seems to linearly increase $\bar{\varepsilon}$, with no signs of asymptotic convergence. This is in contrast with the simulations at higher viscosity of 16 mm^2/s, where grid convergence was observed (Fig. 3A). This convergence is expected from a well-behaved numerical method as the discretization errors approach zero.

This grid dependency study demonstrated that the LB-ILES method does not converge at low viscosities under acoustic scaling ($\Delta t \propto \Delta x$) as done in Fig. 3, where Δt was based on a constant Courant number of 0.01. This Courant-Friedrichs-Lewy (CFL) condition is commonly used in Finite Volume methods as it is directly tied to numerical stability. However, this is not the case for LB methods as stability is governed by the choice of relaxation rate parameters. The disadvantage of using acoustic scaling with LB methods is that the lattice Mach number (Ma_l) remains constant and therefore compressibility errors are not diminished when refining the grid. Consequently, if Ma_l is not sufficiently small, these compressibility errors might dominate as $\Delta x \to 0$, which could hinder convergence. The LB method does converge to the incompressible Navier-Stokes equation if the time step is scaled proportionally to the square of the grid spacing ($\Delta t \propto \Delta x^2$) [34]. This is called diffusive scaling and is equal to scaling the Mach number ($Ma \to 0$). For most of our grid refinement studies, we decided to apply acoustic scaling since Geier et al. [38] showed little difference between acoustic and diffusive scaling when applying the cumulant LB method on a three-dimensional Taylor-Green vortex problem with $Re = 1600$. Acoustic scaling is then advantageous, as it takes less computational time compared to diffusive scaling. However, as depicted in Fig. 3B and C, we observed a grid dependence for our simulations regarding $\bar{\varepsilon}$ when applying acoustic scaling at low viscosities ($Re > 20,000$).

We therefore tested whether diffusive scaling would result in grid convergence, ensuring any compressibility effects are diminished, at a viscosity of 1 mm^2/s where $Re \approx 20,000$. Nevertheless, grid convergence was still not observed (Fig. 4A). This suggests that the behavior of the LB-ILES method's truncation errors is sensitive to the chosen combination of Δt and Δx at low viscosities. The sensitivity to the chosen Δt at fixed Δx of 281 μm was confirmed, where the simulation even seemed to diverge at very small Δt (Fig. 4B). The influence of the lattice spacing Δx at fixed Δt on the truncation errors using $\bar{\varepsilon}$ is more difficult to assess individually, as it cannot be decoupled from resolving smaller scales and thus resolving more ε. In general, a solution depending on the choice of Δx and Δt is undesirable for a numerical method. Yet, for an implicit large eddy simulation (ILES) turbulence model this is not completely surprising behavior, given that the truncation errors are being used to introduce sub-grid dissipation, which are inherently dependent on the chosen Δx and Δt.

The ratio of the grid spacing to the Kolmogorov length scale ($\frac{\Delta x}{\lambda k}$) gives an indication of how much of the flow is simulated explicitly. This

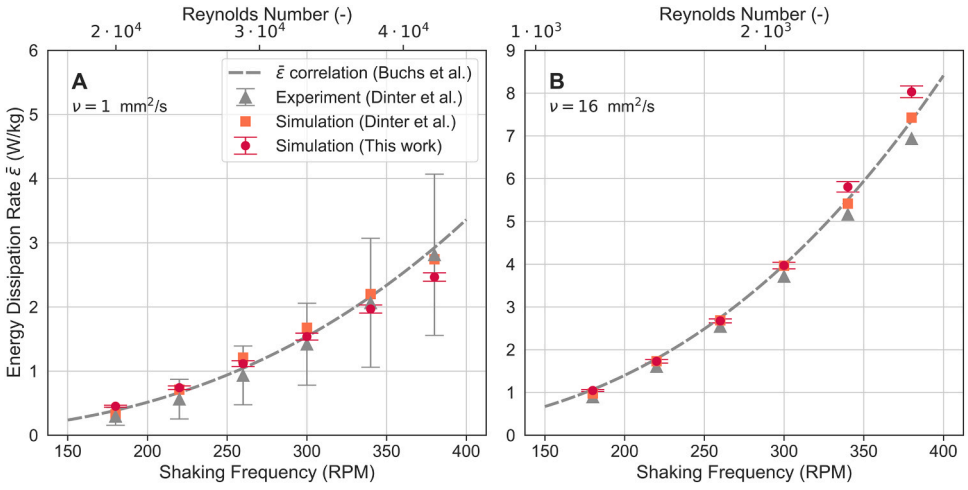

Fig. 2. Comparison LB-ILES mean energy dissipation rate (circles) with volumetric power input measurements performed by Dinter et al. [23] (triangles), Finite Volume (FV) k-omega SST simulations from Dinter et al. [23] (squares) and empirical correlation by Büchs et al. [43] (dotted line). The error bars of our simulations originate from the inherent transient nature of the LB-LES method and represent the ± 2σ confidence interval. The error bars of the data of Dinter et al. [23] correspond to the reported ± 2σ confidence interval with $N = 4$ (only available for $\nu = 1$ mm^2/s). The fluid flow in a 250 mL shake flask was simulated with a filling volume of 25 mL (10 % WV), shaking diameter of 25 mm, surface tension of 0.07 N/m, contact angle of 20 degrees was simulated for a fluid kinematic viscosity ν of both 1 mm^2/s (A) and 16 mm^2/s (B). A lattice spacing of Δx of 211 μm was used (corresponding to 400 lattice points across the shake flask diameter in the x-direction), where Δt was set using a Courant number of 0.01.

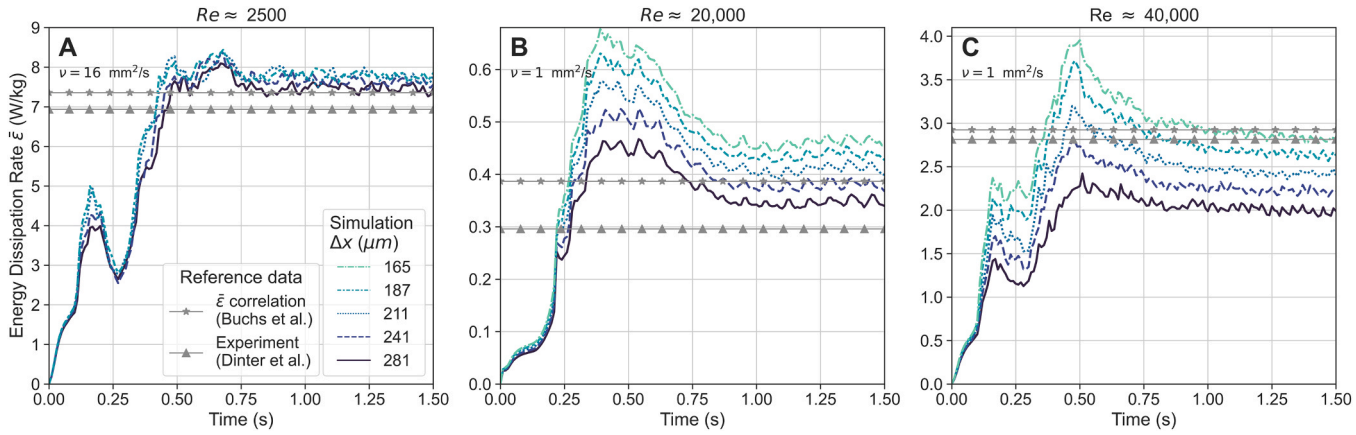

Fig. 3. Grid dependence studies at $Re \approx 2500$ (A, $\nu = 16$ mm^2/s), $Re \approx 20,000$ (B, $\nu = 1$ mm^2/s) and $Re \approx 40,000$ (C, $\nu = 1$ mm^2/s) under acoustic scaling ($\Delta t \propto \Delta x$). Reference data includes measured volumetric power input measurements by [23] (triangles) and empirical correlation by Büchs et al. [43] (stars). Lattice spacings Δx between 281 and 165 μm were used, which correspond to grids between 300 and 500 lattice points across the shake flask diameter, with a constant Courant number of 0.01.

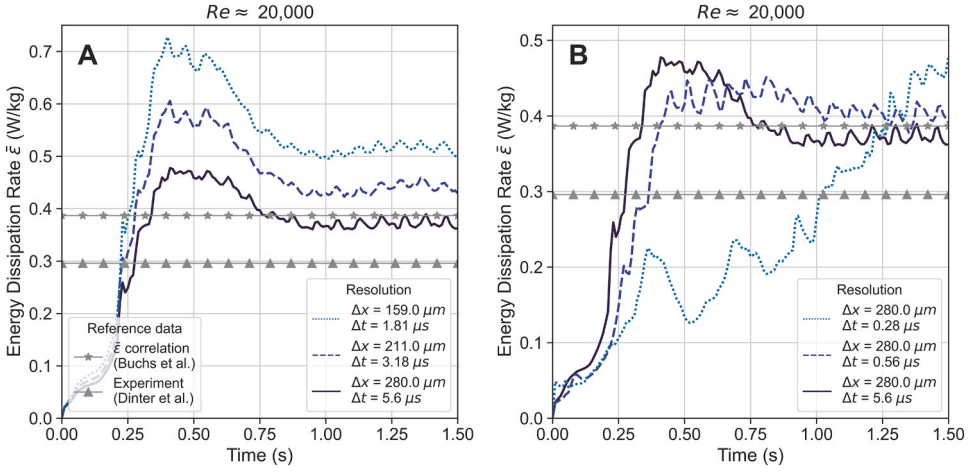

Fig. 4. Grid and time step dependency studies at $Re \approx 20,000$. (A): Grid dependency study under diffusive scaling ($\Delta t \propto \Delta x^2$), at resolutions $\Delta x = 280$ μm, $\Delta t = 5.60$ μs (solid line); $\Delta x = 211$ μm, $\Delta t = 3.18$ μs (dashed line); and $\Delta x = 159$ μm, $\Delta t = 1.81$ μs (dotted line). (B): Time step sensitivity at fixed $\Delta x = 280$ μm with time steps $\Delta t = 5.6$ μs (solid line), $\Delta t = 0.56$ μs (dashed line), and $\Delta t = 5.6$ μs (solid line). Reference data includes measured volumetric power input measurements by [23] (triangles) and empirical correlation by Büchs et al. [43] (stars).

is only an approximation as we used the simulated energy dissipation rate ε to determine the local Kolmogorov length scales, which could differ from the actual local ε. Nevertheless, given that $\bar{\varepsilon}$ was approximated well at a Δx of 211 μm as shown in Fig. 2, the $\frac{\Delta x}{\lambda_k}$ should serve as a good approximation of the local degree of flow that is being resolved. At a Δx of 211 μm and $Re \approx 2500$, the local $\frac{\Delta x}{\lambda_k}$ ratio showed that the simulation is moderately under-resolved where the Δx is maximum 6 times higher than the local λ_k (Fig. 5A). These under-resolved zones primarily occur close to the shake flask wall. At $Re \approx 20,000$ and $Re \approx 40,000$ the simulations become more under-resolved where $\frac{\Delta x}{\lambda_k}$ reaches up to 16 and 24, respectively (Fig. 5B and 5C). Despite the increased under-resolution, the LB-ILES method remained stable. This shows that the used LB-ILES method is robust at dissipating energy using the numerical truncation errors as substitute for sub-grid scale dissipation even at significant under-resolution.

Overall, we showed that for wide variety of spatial resolutions (Δx between 281 and 165 μm) the simulated $\bar{\varepsilon}$ is at least within 50 % of the reference data for a wide range of Reynolds numbers (Re = 1250–40,000). By setting Δx to 211 μm the truncation errors of the LB-ILES method were best controlled and close alignment to the reference data was obtained (Fig. 2). Although it is generally considered bad practice to use a grid resolution that fits the data best, for ILES methods it is more justifiable given the inherent link between truncation errors and spatio-temporal resolution. We acknowledge that the two-phase LB-ILES methods needs further development to improve the use of numerical truncation errors as source for artificial dissipation, given the observed dependence on the chosen spatial and temporal resolution. For the goal of this work, based on the comparison to the reference shake flask data of [23], we assume that given a good agreement in $\bar{\varepsilon}$, the simulations are sufficiently accurate to comment on the hydrodynamic stress distributions in a 125 mL shake flask, under the condition that an appropriate spatial and temporal resolution is used.

3.2. LB-LES model validation of 125 mL shake flask

Given that the correlation of Büchs et al. [43] accurately describes the $\bar{\varepsilon}$ compared to the experimental and simulation data for the 250 mL shake flask, we also compared this correlation to our simulations of the smaller 125 mL shake flask (Fig. 6). For the simulation resolution, 400 lattice points across the shake flask diameter were used ($\Delta x = 160$ μm) with a Courant number of 0.01. This is the same relative number of lattice points used as for the 250 mL shake flask. Again, the LB-ILES method aligns closely to the $\bar{\varepsilon}$ predicted by the correlation, with an

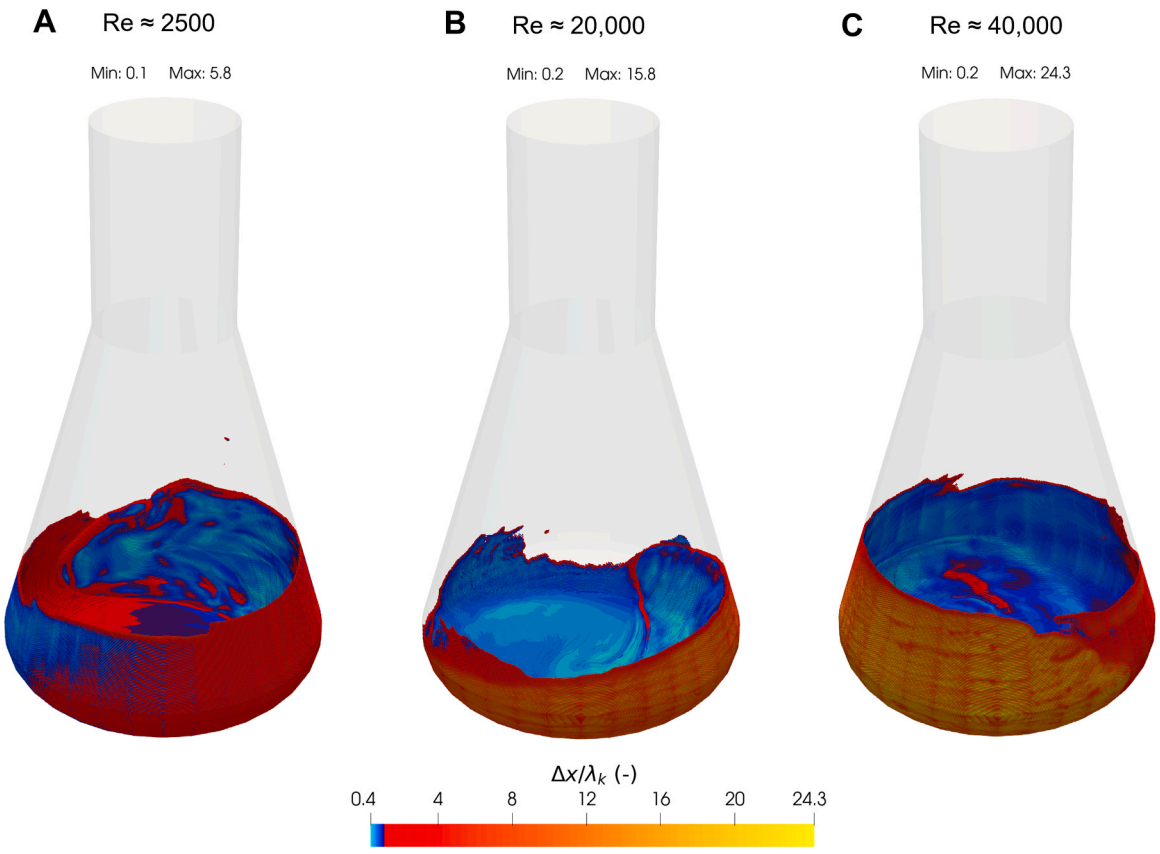

Fig. 5. Ratio of lattice spacing Δx to Kolmogorov length scale λ_k at $Re \approx 2500$ (A, $\nu = 16$ mm^2/s), $Re \approx 20,000$ (B, $\nu = 1$ mm^2/s) and $Re \approx 40,000$ (C, $\nu = 1$ mm^2/s). For these simulations, a Δx of 211 μm was used (400 lattice points across shake flask diameter) with a Courant number of 0.01. Color bar represents the $\frac{\Delta x}{\lambda_k}$-ratio where the midpoint has been set at 1.0, meaning blue zones represent fully resolved flow zones ($\Delta x < \lambda_k$) and red zones represent under-resolved flow zones ($\Delta x > \lambda_k$).

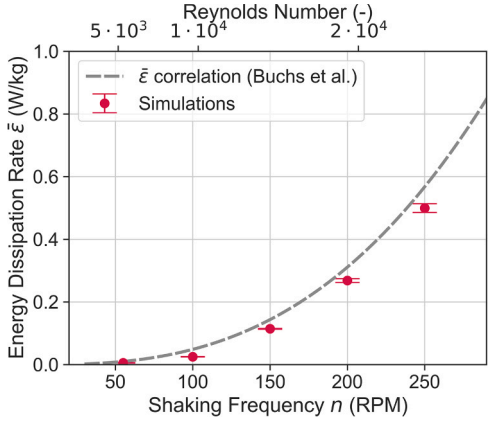

Fig. 6. Comparison LB-ILES mean energy dissipation rate $\bar{\varepsilon}$ (circles) with empirical correlation by Büchs et al. [43]. A 125 mL shake flask with a filling volume of 12.5 mL (10 % WV), shaking diameter of 19 mm, surface tension of 0.07 N/m and fluid kinematic viscosity of 0.7 mm^2/s (T = 37°C) was used for this comparison. A lattice spacing of Δx of 160 μm was used (corresponding to 400 lattice points across the shake flask diameter in the x-direction), where Δt was set using a Courant number of 0.01.

average deviation of 0.034 W/kg (relative deviation of 27.8 %). Some deviation from the correlation of Büchs et al. [43] was expected as this correlation was developed based on data from shaking diameters between 25 and 50 mm, whereas the shaking diameter used here was 19 mm. This probably resulted in slightly different shaking conditions than investigated by Büchs et al. [43].

In addition to the simulation validation using an empirical correlation, a qualitative validation of the 125 mL shake flask simulations was performed by comparing the simulated liquid distributions with experimental liquid distributions (Fig. 7). As the shaking frequency increases, part of the bulk fluid will start rolling along the sides of the shake flask, while the remaining part of the bulk remains relatively stationary on the bottom of the flask. This characteristic fluid behavior is captured by our LB-ILES model.

3.3. Hydrodynamic stress characterization - shear stresses

Understanding how the shaking frequency influences hydrodynamic stresses inside 125 mL shake flasks is important given the shear-sensitivity of stem cells, and in order to be able to use small shake flasks to design hydrodynamic stress scale-down experiments. Fig. 8 shows the time-averaged and shear stress (τ) distributions for shaking frequencies between 55 and 250 rpm ($Re \approx$ 5,000 to 25,000). From 55–250 rpm, the mean shear stress $\bar{\tau}$ increases from around 0.01–0.24 Pa and the shear stress is approximately log-normally distributed. At frequencies above 100 rpm, the distribution appears to become bi-modal, as an additional local maximum is visible on the right side of the distribution. This region of high shear stress values is related to the change in liquid distribution as observed in Fig. 7. Here, the part of the bulk liquid that rolls over the shake flask walls, especially the tip, travels at significantly higher velocities than the rest of the bulk liquid, resulting in higher shear stress values compared to the rest of the bulk liquid.

Fig. 8 also shows reported shear stress thresholds (vertical lines) that influence the differentiation or cultivation of embryonic stem cells (ESC) and embryoid bodies (EB). A shaking frequency higher then 100 rpm

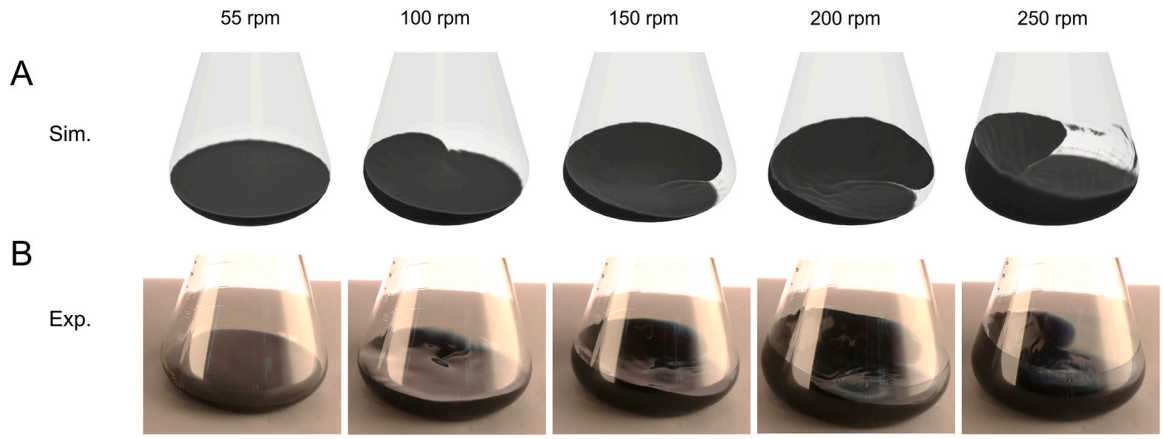

Fig. 7. Comparison of LB-ILES simulated (A) and experimental (B) liquid distributions in a shake flask. A 125 mL shake flask with a filling volume of 12.5 mL (10 % WV), shaking diameter of 19 mm, surface tension of 0.07 N/m and fluid kinematic viscosity of 0.7 mm^2/s (T = 37°C) was used for this comparison.

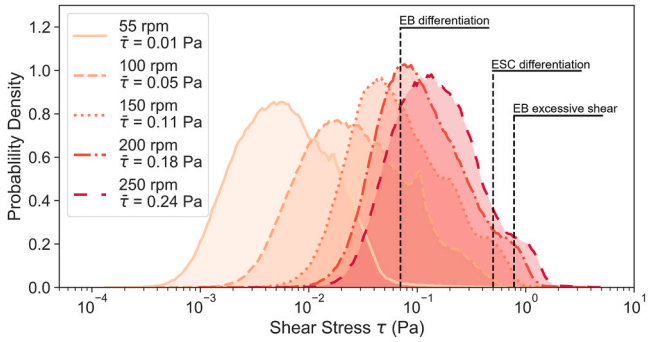

Fig. 8. Shear stress distributions inside the shake flask. Multiple shaking frequencies are compared, including 55 rpm (solid line), 100 rpm (dashed line), 150 rpm (dotted line), 200 rpm (dash-dot line) and 250 rpm (loosely dashed line). Shear stress distributions represent the time-average for 2 shake flask rotations with 8 sample points per rotation. Average shear stress $\bar{\tau}$ is included in the legend. Vertical dotted lines represent known shear stress values that affect stem cell growth and differentiation: modulation of embryoid body (EB) size and structure at 0.07 Pa [44], increased expression of endothelial markers in EBs after exposing embryoid stem cells (ESC) to a shear stress of 0.5 Pa [45], excessive shear completely inhibiting EB formation at 0.78 Pa [46]. A 125 mL shake flask with a filling volume of 12.5 mL (10 % WV), shaking diameter of 19 mm, surface tension of 0.07 N/m and fluid kinematic viscosity of 0.7 mm^2/s (T = 37°C) was used for this comparison.

would result sufficient shear stress to modulate EB size and structure, based on the reported average shear stress of 0.07 Pa by Sargent et al. [44]. Furthermore, Nsiah et al. [45] showed that subjecting ESC monolayers to a constant shear stress of 0.5 Pa for 48 h before initiating EB formation significantly increased the expression of endothelial marker genes and the organization of endothelial cells in EBs. Although the shear stress in a shake flask is not constant, EBs would be exposed to values of 0.5 Pa when the shaking frequencies increases sufficiently. At 150 rpm, 3.1 % of the shake flask volume contains shear stress values about 0.5 Pa, which increases for 200 rpm to 7.0 % and for 250 rpm to 10.8 %. Cormier et al. [46] reported a maximum shear stress of 0.78 Pa during EB bioreactor cultivation, which resulted in excessive shear completely inhibiting EB formation and proliferation. According to our simulations, this maximum shear stress is already reached for all investigated shaking frequencies (Table 1). Although shaken bioreactors are often associated with low shear stress [11], our shake flask simulations show that comparable levels of shear stress may be reached as in lab-scale stirred-tank bioreactors [46]. Furthermore, Table 1 shows that comparable levels of maximum shear stress τ_{max} are reached in our shake flask at high shaking frequency (5.72 Pa at 250 rpm) as found by

Table 1
Summary statistics of shear stress τ and energy dissipation rate ε distributions. Both the absolute τ_{max} and the mean of the 99.9th percentile highest τ values are reported due to the sensitivity of τ_{max} to numerical inaccuracies. Staistics represent the time-average for 2 shake flask rotations with 8 sample points per rotation. A 125 mL shake flask with a filling volume of 12.5 mL (10 % WV), shaking diameter of 19 mm, surface tension of 0.07 N/m and fluid kinematic viscosity of 0.7 mm^2/s (T = 37°C) was used for this comparison.

Shaking frequency rpm	$\bar{\tau}$ Pa	$\tau_{max,99}$ Pa	τ_{max} Pa	$\bar{\varepsilon}$ W/kg	$\varepsilon_{max}/\bar{\varepsilon}$ [–]
55	0.01	0.79	3.10	0.005	14,499
100	0.05	0.81	2.53	0.025	1793
150	0.11	1.34	3.68	0.114	637
200	0.18	2.08	4.95	0.268	298
250	0.24	2.88	5.72	0.500	212

Šrom et al. [31], who reported values of around 6.5 Pa in a 3 L bioreactor using their shear sensitive micro-probe experiments and CFD simulations. However, compared at the same specific power input (P/V) of 0.35 W/kg, which corresponds to approximately a shaking frequency of 100 rpm in a shake flask, the τ_{max} of the shake flask is approximately half compared to the 3 L bioreactor used by Šrom et al. [31]. This is in consensus with the general believe that the hydrodynamic heterogeneity in shake flasks is lower compared to stirred-tank bioreactors [24].

Similar to Šrom et al. [31], we reported the $\varepsilon_{max}/\bar{\varepsilon}$ ratio as a measure for hydrodynamic heterogeneity (Table 1). Although the $\varepsilon_{max}/\bar{\varepsilon}$ ratios for the shake flask are generally lower than compared to the work of Šrom et al. [31] (1100 for lab-scale and 4000 for large-scale bioreactors), at lower shaking frequencies $\varepsilon_{max}/\bar{\varepsilon}$ becomes unexpectedly high (≈ 1800 for 100 rpm and ≈ 14,000 for 55 rpm). This highlights a challenge in determining this ratio from CFD simulations, as it is based on a single absolute maximum ε_{max} which is susceptible to numerical inaccuracies. Especially for the two-phase LB-ILES method used in this work, where stability is a major challenge, such maxima become unreliable. Consequently, comparing $\varepsilon_{max}/\bar{\varepsilon}$ between different simulation methods is challenging as it now also depends on the stability and consistency of the numerical method. For example, Liu et al. [24] recognized this challenge and defined ε_{max} based on the mean of the top 1 percent of highest values (99th percentile), which is why we reported, in a similar fashion, $\tau_{max,99}$. However, determining where to set this cutoff remains rather arbitrary and no consensus on this definition exists. Thus, although conceptually hydrodynamic stress parameters based on maximum values (e.g,. τ_{max} and ε_{max}) are sensible, defining them using simulations is not straightforward.

3.4. Hydrodynamic stress characterization - Kolmogorov length scales

EBs are large compared to single stem cells and have been shown to grow up to 400 μm in diameter [6,47]. The local fluid shear stress is no longer an adequate measure of hydrodynamic stress as these aggregates no longer follow local flow patterns. Rather, turbulent eddies smaller than the aggregate size with sufficient energy are hypothesized to be damaging to these cell aggregates. The size of the smallest turbulent eddies can be estimated using the Kolmogorov length scale λ_k (Equation (18)). A typical rule-of-thumb to determine whether the turbulent eddies are damaging originates from the work of Croughan et al. [9], who found detrimental effects on cell viability if the average Kolmogorov length scale $\overline{\lambda}_k$ falls below two-thirds of the aggregate size. Fig. 9 shows the distribution of λ_k inside the shake flask for a range of shaking frequencies. Also shown are the average sizes of single ESCs (15 μm), microcarriers (170 μm) and EBs (400 μm) [47]. For microcarrier cultivations, more than 51 % of the volume contains eddies smaller than two-thirds of the microcarrier size when increasing the shaking frequency above 100 rpm. For EBs of 400 μm, this volume reaches 97 % when shaking increases above 100 rpm. This is in line with the notion that microcarrier cultivations are conducted at low shaking speeds ($<$ 55 rpm) [44]. Yet, even at a shaking frequency of 55 rpm, our simulations predict significant volume fraction containing eddy sizes below two-thirds of microcarriers and EBs (volume fractions of 7.3 % and 89 % respectively), even though successful EB cultivation at comparable hydrodynamic conditions have been shown [44,46]. As expected, for single ESCs, the $\overline{\lambda}_k$ is significantly larger than the average cell size for all shaking frequencies (volume fractions less than 0.01 %).

4. Discussion

With the current simulation setup, we observe good overall predictions for energy dissipation for a range of different shaking conditions, provided an appropriate selection for the grid and time step size. In general, a dependency on simulation parameters, such as grid and time step size, is undesirable for a numerical method as these parameters are unrelated to the underlying fluid flow physics. The observed grid dependencies were unexpected, especially under the rather strict diffusive scaling of the simulations. Our results showed no apparent difference in grid dependence between acoustic and diffusive scaling, indicating that numerical compressibility errors were likely not the cause of the grid dependence. For simulations of biotechnologically relevant fluids, acoustic scaling will diminish any numerical compressibility effects if a sufficiently low Courant number is selected.

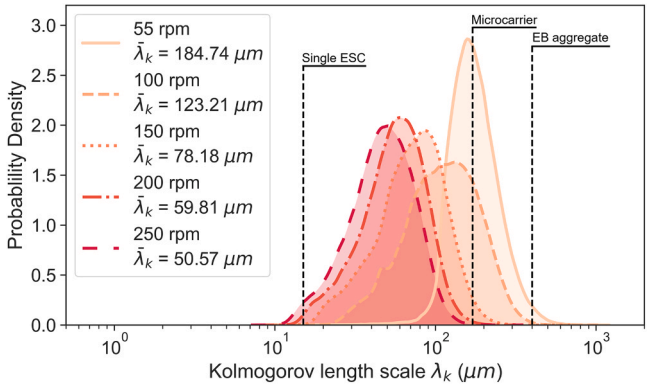

Fig. 9. Kolmogorov length scale (λ_k) distributions inside the shake flask. Multiple shaking frequencies are compared, including 55 rpm (solid line), 100 rpm (dashed line), 150 rpm (dotted line), 200 rpm (dash-dot line) and 250 rpm (loosely dashed line). Kolmogorov length scale distributions represent the time-average for two shake flask rotations with 8 sample points per rotation. Average Kolmogorov length scale ($\overline{\lambda_k}$) is included in the legend. Vertical dotted lines represent average size of single embryoid stem cells (ESC) of 15 μm, average size of microcarriers of 170 μm, and embryoid body (EB) size of 400 μm as reported by [47]. A 125 mL shake flask with a filling volume of 12.5 mL (10 % WV), shaking diameter of 19 mm, surface tension of 0.07 N/m and fluid kinematic viscosity of 0.7 mm^2/s (T = 37°C) was used for this comparison.

One possibility explaining this grid dependence is the used boundary condition at the shake flask wall, where a rather simplistic grid-aligned half-way bounce-back boundary was used to enforce the no-slip condition. For curved surfaces, such as the shake flask wall, this grid-aligned representation leads to so-called staircasing resulting in geometrical inaccuracies. Furthermore, at low viscosities, the velocity boundary layer becomes thinner making it more difficult to accurately resolve steep gradients, especially during simulations at higher Reynolds numbers when the flow close to the wall is significantly under-resolved ($\Delta x >> \lambda_k$). Another consequence of staircasing is that the half-way bounce-back scheme effectively becomes first-order accurate [48]. This is in contrast to the order of accuracy of the LB methods themselves, which are at least second-order accurate, or in the case of the cumulant LB method as used here, even higher-order accurate [36]. Consequently, numerical errors introduced by the boundary representation might not diminish sufficiently, or not diminish at all, when refining the grid. This could potentially also degrade the accuracy of the simulated bulk fluid and result in an apparent grid dependence. This boundary representation is especially critical when modeling shake flask fluid flow, as the fluid motion is introduced through the friction with the shake flask wall. By improving the boundary representation to, for example, interpolated bounce-back schemes the geometrical errors could be reduced and a higher-order accuracy could be achieved, thereby improving grid convergence [48].

The apparent grid and time step dependency also raises the question whether such implicit large eddy simulations (ILES) are desired over the more conventional explicit large eddy simulations (LES) when using two-phase LB methods. With ILES, the sub-grid dissipation is controlled by rather heuristic model parameters, such as higher-order relaxation rate limiters, and velocity and pressure field filter parameters. Although some of these parameters have been tuned using reference data, for example by Geier et al. [36] and Sitompul and Aoki [33], some of these are still free parameters that were set solely based on good stability properties. Further tuning of these parameters using experimental or DNS results might improve the accuracy of LB-ILES simulations. This is opposite to explicit LES, which usually only involves one free parameter for which the value is determined based on DNS results for various flow problems [49]. Coupling two-phase LB methods with explicit LES models might improve the accuracy of the simulated dissipation. However, Geier et al. [38] showed that for a single-phase cumulant LB method with a Wall Adaptive Local Eddy (WALE) model the simulation accuracy and efficiency decreased at a moderate Reynolds number of 1600, compared to using the relaxation rate limiters of the cumulant LB scheme to introduce the sub-grid dissipation (ILES). It is thus still an open question whether adding an explicit LES model would improve the simulated energy dissipation for shake flask simulations. In any case, when applying two-phase LB-ILES methods, we strongly recommend to thoroughly assess the grid and time step dependencies, as well as carefully validating the simulation results using quantitative reference data.

We used our shake flask simulations to quantify shear stress distributions for different shaking frequencies, and related those to reported stress responses of embryonic stem cells (ESC) and embryoid bodies (EB). In most of these cases, reported stress values are based on an underlying assumption about how the stress is related to the observed cell response. For example, Sargent et al. [44] related the average shear stress to EB response, whereas Nsiah et al. [45] only reported the maximum shear stress. It is however not always obvious which shear stress (e.g., mean or maximum) metric correlates best with actual cellular responses. Similar limitations exist when using the Kolmogorov length scale λ_k to determine whether hydrodynamic conditions are damaging to suspended 3D cell aggregates. The rule-of-thumb defined

by Croughan et al. [9] states that the hydrodynamics become significantly damaging if the λ_k falls below two-thirds of the aggregate size, is still widely used. However, the relation of this length scale to an actual cell death rate k_d is still highly cell type and microcarrier material specific. Using this rule-of-thumb, our simulations would suggest that shaking the 125 mL shake flask at 55 rpm would result in hydrodynamic damaging conditions for EB cultivation. Yet, EBs have been successfully cultivated in such hydrodynamic conditions [39,46]. Therefore, experiments are needed to determine the exact relation between k_d and λ_k to really understand how different cultivation systems and operating conditions affect EB growth.

Furthermore, hydrodynamic stress parameters, such as the average and maximum shear stress, do not include any temporal information, such as exposure duration or exposure frequency to certain shear stress thresholds. For instance, Bratengeier et al. [50] showed that not just the maximum shear stress, but rather the combination of a certain amplitude and duration of the shear stress stimulus results in a strong cellular response of the mechanosensitive Piezo1 receptor by hematopoeietic progenitor cells. The notion that damage results from a combination of stress magnitude and exposure duration is consistent with prior experiments on fungal agglomerates in stirred vessels, where the impact was best captured by the so-called Energy Dissipation Circulation Function [51]. Experiments on ESCs and EBs as performed by Bratengeier et al. [50] would be helpful future research to better understand the relation between cell response and nature of shear stress.

The advantage of the LB-ILES method of M-Star CFD used here is its inherent transient nature. Compared to traditional Reynolds-averaged Navier-Stokes (RANS) based approaches, which only yields a time-averaged representation of turbulence, the LB-LES inherently simulates the temporal fluctuations in the fluid flow including fluctuations in the hydrodynamic stresses. Simulation techniques such as lifeline analysis, where computational (Lagrangian) particles are tracked during a CFD simulation to obtain a collection of time-series that represent the physical conditions (e.g., shear stress) encountered by cells, would allow the quantification of exposure duration and frequency to certain shear stress thresholds [30]. Since M-Star's LBM solver runs naively on the GPU, longer time-scale simulations (minutes, hours) including Lagrangian particle tracking, are now tractable on simple desktop hardware. We do note, however, that M-Star's two-phase LB-ILES is computationally more demanding than M-Star's single-phase models due to the required larger velocity set (D3Q27), the use of a cumulant LB collision operator, and additional phase-field equations that must be solved. Therefore, the computational time is not yet as low as in stirred-tank bioreactor simulations as, for example, reported by Haringa [30]. In the present work, an emphasis was placed on first validating the LB-ILES approach, which was followed up with a straightforward analysis of the time-averaged shear stress and Kolmogorov length scale distributions. In future work, we will explore the potential of LB-ILES for simulating lifelines to quantify exposure time and frequency to certain hydrodynamic stress thresholds in the context of stem cell cultures.

5. Conclusion

The sensitivity of stem cells to hydrodynamic stress is a major challenge when developing stem cell therapy-based production processes. Specifically, the hydrodynamic differences between lab-scale and production-scale cultivation systems makes scale-up of the production process challenging. Quantifying the hydrodynamic stresses in lab-scale systems, such as shake flasks, improves process understanding and helps develop low-cost scale-down experiments to approximate hydrodynamic stresses in larger cultivation systems, such as stirred-tank bioreactors. We used the LB-ILES method of M-Star CFD to simulate a 125 mL shake flask and quantify the shear stress and Kolmogorov length scales distributions inside the system.

First, we showed good overall predictions of the LB-ILES method for energy dissipation in 250 mL shake flasks by comparing our results to reported experimental and simulation values. However, some challenges were identified with the LB-ILES method, specifically regarding grid and time step dependencies, which is why we stress the importance of validation when using such methods. With appropriate simulation settings, the accuracy of the 125 mL shake flask model was assessed using an empirical correlation for volumetric power input and experimental liquid distribution data.

The mean shear stress in our shake flask setup (19 mm shaking diameter, 10 % working volume) increases from 0.01 P to 0.24 Pa when increasing the shaking frequency from 55 to 250 rpm. At higher shaking frequencies, maximum shear stresses (5.72 Pa at 250 rpm) comparable to 3 L lab-scale bioreactors are achieved, showcasing the potential of small shake flasks to mimic larger cultivation systems. Compared to reported values in literature, the 125 mL shake flask can generate sufficient shear stress to affect gene expression in embryoid bodies (EB), or even result in excessive shear damage on EBs. Similarly, the mean Kolmogorov length scale decreases from 185 to 51 μm when increasing the shaking frequency from 55 to 250 rpm. Although our simulations predict a significant volume fraction at low shaking frequency (89 % at 55 rpm) that contain eddies with sufficient energy to be damaging to EBs (reported size of 400 μm), the rule-of-thumb by Croughan et al. [9] requires case-specific refinement and experiments are needed to determine the exact relation between Kolmogorov length scale and shear damage.

Computational fluid dynamic simulation methods, as used in this work, are useful to determine hydrodynamic stresses to which stem cells and EBs are subjected during cultivation. Our shake flask model can be used to design scale-down experiments, by tuning the shake flask operating conditions (e.g., shaking frequency) to mimic hydrodynamic stress conditions of large-scale cultivation systems, allowing for easier and cheaper experimentation. Ultimately, such scale-down experiments designed using our shake flask simulations can help guide scale-up of stem cell culture production processes.

CRediT authorship contribution statement

Ramon D. van Valderen: Writing – review & editing, Writing – original draft, Visualization, Validation, Methodology, Investigation, Formal analysis, Data curation, Conceptualization. **Brenda E. Juarez-Garza:** Writing – review & editing, Investigation. **Marieke E. Klijn:** Writing – review & editing, Supervision, Funding acquisition. **Marcel Ottens:** Writing – review & editing, Supervision, Funding acquisition. **Cees Haringa:** Writing – review & editing, Supervision, Funding acquisition, Conceptualization.

Declaration of Competing Interest

The authors declare that they have no known competing financial interests or personal relationships that could have appeared to influence the work reported in this paper.

Data availability

The data that support the findings of this study are available from the corresponding author upon reasonable request.

Acknowledgements

This work was performed within the TRACER consortium, which is funded by the ZonMw PSIDER programme (grant number 10250022110001). The staff of M-STAR CFD, in particular Johannes Wutz and Brian Devincentis, are thanked for their support. Also Jochen Büchs and Carl Dinter are thanked for sharing their experimental and computational results, and Sasha Szkudlarek for the useful discussion on LBM. The authors are grateful to colleagues from the TRACER consortium and the department of Biotechnology from TUD for their

valuable discussions.

Appendix A. Supporting information

Supplementary data associated with this article can be found in the online version at doi:10.1016/j.bej.2025.109734.

References

[1] R.M. Aly, Current state of stem cell-based therapies: an overview, Stem Cell Investig. 7 (2020) 8, https://doi.org/10.21037/sci-2020-001.

[2] S. Yamanaka, Pluripotent stem cell-based cell therapy—promise and challenges, Cell Stem Cell 27 (2020) 523–531, https://doi.org/10.1016/j.stem.2020.09.014.

[3] S. Demirci, A. Leonard, J.F. Tisdale, Hematopoietic stem cells from pluripotent stem cells: clinical potential, challenges, and future perspectives, Stem Cells Transl. Med. 9 (2020) 1549–1557, https://doi.org/10.1002/sctm.20-0247.

[4] S. Jung, K.M. Panchalingam, R.D. Wuerth, L. Rosenberg, L.A. Behie, Large-scale production of human mesenchymal stem cells for clinical applications, Biotechnol. Appl. Biochem. 59 (2012) 106–120, https://doi.org/10.1002/bab.1006.

[5] G. Pettinato, X. Wen, N. Zhang, Engineering strategies for the formation of embryoid bodies from human pluripotent stem cells, Stem Cells Dev. 24 (2015) 1595–1609, https://doi.org/10.1089/scd.2014.0427.

[6] C. Bernecker, M. Ackermann, N. Lachmann, L. Rohrhofer, H. Zaehres, M.J. Araúzo-Bravo, E. van den Akker, P. Schlenke, I. Dorn, Enhanced ex vivo generation of erythroid cells from human induced pluripotent stem cells in a simplified cell culture system with low cytokine support, Stem Cells Dev. 28 (2019) 1540–1551, https://doi.org/10.1089/scd.2019.0132.

[7] K.M. Panchalingam, S. Jung, L. Rosenberg, L.A. Behie, Bioprocessing strategies for the large-scale production of human mesenchymal stem cells: a review, Stem Cell Res. Ther. 6 (2015) 225, https://doi.org/10.1186/s13287-015-0228-5.

[8] A. Humphrey, Shake flask to fermentor: what have we learned? Biotechnol. Prog. 14 (1998) 3–7, https://doi.org/10.1021/bp970130k.

[9] M.S. Croughan, J.-F. Hamel, D.I.C. Wang, Hydrodynamic effects on animal cells grown in microcarrier cultures, Biotechnol. Bioeng. 29 (1987) 130–141, https://doi.org/10.1002/bit.260290117.

[10] A.M. de Soure, A. Fernandes-Platzgummer, C.L. daSilva, J.M.S. Cabral, Scalable microcarrier-based manufacturing of mesenchymal stem/stromal cells, J. Biotechnol. 236 (2016) 88–109, https://doi.org/10.1016/j.jbiotec.2016.08.007.

[11] C.F. Bellani, J. Ajeian, L. Duffy, M. Miotto, L. Groenewegen, C.J. Connon, Scale-up technologies for the manufacture of adherent cells, Front. Nutr. 7 (2020), https://doi.org/10.3389/fnut.2020.575146.

[12] M.J. Jenkins, S.S. Farid, Human pluripotent stem cell-derived products: advances towards robust, scalable and cost-effective manufacturing strategies, Biotechnol. J. 10 (2015) 83–95, https://doi.org/10.1002/biot.201400348.

[13] W. Zeng, L. Guo, S. Xu, J. Chen, J. Zhou, High-throughput screening technology in industrial biotechnology, Trends Biotechnol. 38 (2020) 888–906, https://doi.org/10.1016/j.tibtech.2020.01.001.

[14] F. Aglialoro, A. Abay, N. Yagci, M.A.E. Rab, L. Kaestner, R. Van Wijk, M. VonLindern, E. Van Den Akker, Mechanical stress induces Ca2+ -dependent signal transduction in erythroblasts and modulates erythropoiesis, Int. J. Mol. Sci. 22 (2021) 955, https://doi.org/10.3390/ijms22020955.

[15] J. Büchs, U. Maier, S. Lotter, C.P. Peter, Calculating liquid distribution in shake flasks on rotary shakers at waterlike viscosities, Biochem. Eng. J. 34 (2007) 200–208, https://doi.org/10.1016/j.bej.2006.12.005.

[16] M. Reclari, Hydrodynamics of Orbital Shaken Bioreactors [dissertation], Lausanne: Swiss Federal Institute of Technology in Lausanne (EPFL) (2013), https://doi.org/10.5075/epfl-thesis-5759.

[17] J. Büchs, U. Maier, C. Milbradt, B. Zoels, Power consumption in shaking flasks on rotary shaking machines: I. Power consumption measurement in unbaffled flasks at low liquid viscosity, Biotechnol. Bioeng. 68 (2000) 589–593, https://doi.org/10.1002/(SICI)1097-0290(20000620)68:6< 589::AID-BIT1> 3.0.CO;2-J.

[18] F. Delvigne, R. Takors, R. Mudde, W. van Gulik, H. Noorman, Bioprocess scale-up/down as integrative enabling technology: From fluid mechanics to systems biology and beyond, Microb. Biotechnol. 10 (2017) 1267–1274, https://doi.org/10.1111/1751-7915.12803.

[19] D. Kreitmayer, Computational Fluid Dynamics Simulations of Single-Use Bioreactors for the Scale-Up of, in: Cell Culture Processes [dissertation],, University, Heidelberg: Heidelberg, 2022, https://doi.org/10.11588/heidok.00032116.

[20] O. Šrom, V. Trávníková, J. Wutz, M. Kuschel, A. Unsoeld, T. Wucherpfennig, M. Šoóš, Characterization of hydrodynamic stress in ambr250® bioreactor system and its impact on mammalian cell culture, Biochem. Eng. J. 177 (2022) 108240, https://doi.org/10.1016/j.bej.2021.108240.

[21] C. Li, J.-Y. Xia, J. Chu, Y.-H. Wang, Y.-P. Zhuang, S.-L. Zhang, CFD analysis of the turbulent flow in baffled shake flasks, Biochem. Eng. J. 70 (2013) 140–150, https://doi.org/10.1016/j.bej.2012.10.012.

[22] H. Zhang, W. Williams-Dalson, E. Keshavarz-Moore, P.A. Shamlou, Computational-fluid-dynamics (CFD) analysis of mixing and gas–liquid mass transfer in shake flasks, Biotechnol. Appl. Biochem. 41 (2005) 1–8, https://doi.org/10.1042/BA20040082.

[23] C. Dinter, A. Gumprecht, M.A. Menze, A. Azizan, P.-J. Niehoff, S. Hansen, J. Büchs, Validation of computational fluid dynamics of shake flask experiments at moderate viscosity by liquid distributions and volumetric power inputs, Sci. Rep. 14 (2024) 3658, https://doi.org/10.1038/s41598-024-53980-7.

[24] Y. Liu, Z.-J. Wang, J. Zhang, J.-y. Xia, J. Chu, S.-L. Zhang, Y.-P. Zhuang, Quantitative evaluation of the shear threshold on Carthamus tinctorius L. cell growth with computational fluid dynamics in shaken flask bioreactors, Biochem. Eng. J. 113 (2016) 66–76, https://doi.org/10.1016/j.bej.2016.06.001.

[25] C. Dinter, A. Gumprecht, M.A. Menze, A. Azizan, S. Hansen, J. Büchs, Exploration of the Out-of-Phase Phenomenon in Shake Flasks by CFD Calculations of Volumetric Power Input, kLa Value and Shear Rate at Elevated Viscosity, Biotechnol. Bioeng. n/a (2024), https://doi.org/10.1002/bit.28892.

[26] T. Krüger, H. Kusumaatmaja, A. Kuzmin, O. Shardt, G. Silva, E.M. Viggen, The Lattice Boltzmann Method: Principles and Practice, Graduate Texts in Physics, Springer International Publishing, Cham, 2017, https://doi.org/10.1007/978-3-319-44649-3.

[27] J.A. Thomas, A. Rahman, J. Wutz, Y. Wang, B. DeVincentis, B. McGuire, L. Cao, Modeling free surface gas transfer in agitated lab-scale bioreactors, Chem. Eng. Commun. 210 (2023) 1328–1339, https://doi.org/10.1080/00986445.2022.2084392.

[28] C. Sirasitthichoke, B. Teoman, J. Thomas, P.M. Armenante, Computational prediction of the just-suspended speed, Njs, in stirred vessels using the lattice Boltzmann method (LBM) coupled with a novel mathematical approach, Chem. Eng. Sci. 251 (2022) 117411, https://doi.org/10.1016/j.ces.2021.117411.

[29] C.L. Oliveira, Z. Pace, J.A. Thomas, B. DeVincentis, C. Sirasitthichoke, S. Egan, J. Lee, CFD-based bioreactor model with proportional–integral–derivative controller functionality for dissolved oxygen and pH, Biotechnol. Bioeng. 121 (2024) 655–669, https://doi.org/10.1002/bit.28598.

[30] C. Haringa, An analysis of organism lifelines in an industrial bioreactor using Lattice-Boltzmann CFD, Eng. Life Sci. n/a (2022), https://doi.org/10.1002/elsc.202100159.

[31] O. Šrom, M. Šoóš, M. Kuschel, T. Wucherpfennig, J. Fitschen, M. Schlüter, Study of hydrodynamic stress in cell culture bioreactors via *lattice-Boltzmann CFD* simulations supported by micro-probe shear stress method, Biochem. Eng. J. 208 (2024) 109337, https://doi.org/10.1016/j.bej.2024.109337.

[32] H. Huang, M.C. Sukop, X.-Y. Lu, Multiphase Lattice Boltzmann Methods: Theory and Application, John Wiley and Sons, Inc., Chichester, West Sussex, UK, 2015.

[33] Y.P. Sitompul, T. Aoki, A filtered cumulant lattice Boltzmann method for violent two-phase flows, J. Comput. Phys. 390 (2019) 93–120, https://doi.org/10.1016/j.jcp.2019.04.019.

[34] M. Geier, M. Schönherr, A. Pasquali, M. Krafczyk, The cumulant lattice Boltzmann equation in three dimensions: Theory and validation, Comput. Math. Appl. 70 (2015) 507–547, https://doi.org/10.1016/j.camwa.2015.05.001.

[35] M. Geier, A. Fakhari, T. Lee, Conservative phase-field lattice Boltzmann model for interface tracking equation, Phys. Rev. E 91 (2015) 063309, https://doi.org/10.1103/PhysRevE.91.063309.

[36] M. Geier, A. Pasquali, M. Schönherr, Parametrization of the cumulant lattice Boltzmann method for fourth order accurate diffusion part I: Derivation and validation, J. Comput. Phys. 348 (2017) 862–888, https://doi.org/10.1016/j.jcp.2017.05.040.

[37] F.F. Grinstein, L.G. Margolin, W.J. Rider, Implicit Large Eddy Simulation: Computing Turbulent Fluid Dynamics (Eds.), Cambridge University Press, Cambridge, 2007, https://doi.org/10.1017/CBO9780511618604.

[38] M. Geier, S. Lenz, M. Schönherr, M. Krafczyk, Under-resolved and large eddy simulations of a decaying Taylor–Green vortex with the cumulant lattice Boltzmann method, Theor. Comput. Fluid Dyn. 35 (2021) 169–208, https://doi.org/10.1007/s00162-020-00555-7.

[39] G. Yirme, M. Amit, I. Laevsky, S. Osenberg, J. Itskovitz-Eldor, Establishing a dynamic process for the formation, propagation, and differentiation of human embryoid bodies, Stem Cells Dev. 17 (2008) 1227–1242, https://doi.org/10.1089/scd.2007.0272.

[40] M. Amit, J. Chebath, V. Margulets, I. Laevsky, Y. Miropolsky, K. Shariki, M. Peri, I. Blais, G. Slutsky, M. Revel, J. Itskovitz-Eldor, Suspension culture of undifferentiated human embryonic and induced pluripotent stem cells, Stem Cell Rev. Rep. 6 (2010) 248–259, https://doi.org/10.1007/s12015-010-9149-y.

[41] A. Sahabian, J. Dahlmann, U. Martin, R. Olmer, Production and cryopreservation of definitive endoderm from human pluripotent stem cells under defined and scalable culture conditions, Nat. Protoc. 16 (2021) 1581–1599, https://doi.org/10.1038/s41596-020-00470-5.

[42] P.-H. Chiu, Y.-T. Lin, A conservative phase field method for solving incompressible two-phase flows, J. Comput. Phys. 230 (2011) 185–204, https://doi.org/10.1016/j.jcp.2010.09.021.

[43] J. Büchs, U. Maier, C. Milbradt, B. Zoels, Power consumption in shaking flasks on rotary shaking machines: II. Nondimensional description of specific power consumption and flow regimes in unbaffled flasks at elevated liquid viscosity, Biotechnol. Bioeng. 68 (2000) 594–601, https://doi.org/10.1002/(SICI)1097-0290(20000620)68:6< 594::AID-BIT2> 3.0.CO;2-U.

[44] C.Y. Sargent, G.Y. Berguig, M.A. Kinney, L.A. Hiatt, R.L. Carpenedo, R.E. Berson, T. C. McDevitt, Hydrodynamic modulation of embryonic stem cell differentiation by rotary orbital suspension culture, Biotechnol. Bioeng. 105 (2010) 611–626, https://doi.org/10.1002/bit.22578.

[45] B.A. Nsiah, T. Ahsan, S. Griffiths, M. Cooke, R.M. Nerem, T.C. McDevitt, Fluid shear stress pre-conditioning promotes endothelial morphogenesis of embryonic stem cells within embryoid bodies, Tissue Eng. Part A 20 (2014) 954–965, https://doi.org/10.1089/ten.tea.2013.0243.

[46] J.T. Cormier, N.I.Z. Nieden, D.E. Rancourt, M.S. Kallos, Expansion of undifferentiated murine embryonic stem cells as aggregates in suspension culture

bioreactors, Tissue Eng. 12 (2006) 3233–3245, https://doi.org/10.1089/ten.2006.12.3233.
[47] C.L. Bauwens, R. Peerani, S. Niebruegge, K.A. Woodhouse, E. Kumacheva, M. Husain, P.W. Zandstra, Control of human embryonic stem cell colony and aggregate size heterogeneity influences differentiation trajectories, Stem Cells 26 (2008) 2300–2310, https://doi.org/10.1634/stemcells.2008-0183.
[48] Z.-Q. Dong, L.-P. Wang, C. Peng, T. Chen, A systematic study of hidden errors in the bounce-back scheme and their various effects in the lattice Boltzmann simulation of viscous flows, Phys. Fluids 34 (2022) 093608, https://doi.org/10.1063/5.0106954.
[49] P. Sagaut. Large Eddy Simulation for Incompressible Flows: an Introduction, Scientific Computation, 3rd ed., Springer, Berlin; New York, 2006.
[50] C. Bratengeier, A. Liszka, J. Hoffman, A.D. Bakker, A. Fahlgren, High shear stress amplitude in combination with prolonged stimulus duration determine induction of osteoclast formation by hematopoietic progenitor cells, FASEB J. 34 (2020) 3755–3772, https://doi.org/10.1096/fj.201901458R.
[51] P. Jüsten, G.C. Paul, A.W. Nienow, C.R. Thomas, Dependence of mycelial morphology on impeller type and agitation intensity, Biotechnol. Bioeng. 52 (1996) 672–684, https://doi.org/10.1002/(SICI)1097-0290(19961220)52:63.0.CO;2-L.